Preferential concentration of particles by turbulence

Kyle D. Squires and John K. Eaton

Citation: Physics of Fluids A: Fluid Dynamics (1989-1993) **3**, 1169 (1991); doi: 10.1063/1.858045
View online: http://dx.doi.org/10.1063/1.858045
View Table of Contents: http://scitation.aip.org/content/aip/journal/pofa/3/5?ver=pdfcov
Published by the AIP Publishing

Preferential concentration of particles by turbulence

Kyle D. Squires and John K. Eaton
Department of Mechanical Engineering, Stanford University, Stanford, California 94305

(Received 28 August 1990; accepted 11 December 1990)

Direct numerical simulation of isotropic turbulence was used to investigate the effect of turbulence on the concentration fields of heavy particles. The hydrodynamic field was computed using 64^3 points and a statistically stationary flow was obtained by forcing the low-wave-number components of the velocity field. The particles used in the simulations were time advanced according to Stokes drag law and were also assumed to be much more dense than the fluid. Properties of the particle cloud were obtained by following the trajectories of 1 000 000 particles through the simulated flow fields. Three values of the ratio of the particle time constant to large-scale turbulence time scale were used in the simulations: 0.075, 0.15, and 0.52. The simulations show that the particles collect preferentially in regions of low vorticity and high strain rate. This preferential collection was most pronounced for the intermediate particle time constant (0.15) and it was also found that the instantaneous number density was as much as 25 times the mean value for these simulations. The fact that dense particles collect in regions of low vorticity and high strain in turn implies that turbulence may actually inhibit rather than enhance mixing of particles.

I. INTRODUCTION

The mixing of particles by turbulent flow fields is certainly one of the most interesting problems in fluid mechanics. The range of applications in which particles are transported and mixed by turbulence are as diverse as the dispersion of pollutants in the atmosphere to the pneumatic transport of particles in coal power plants. Aside from the technological relevance of these and other applications, particle motion in turbulent flow fields is also an area of fundamental interest.

There are a number of techniques available by which one may study particle mixing or, more generally, scalar transport. As is well known, Taylor[1] has shown that scalar dispersion in a turbulent fluid lends itself most suitably to a Lagrangian analysis, i.e., an analysis in which one utilizes information obtained along the trajectory of individual particles. Batchelor[2] and Corrsin[3] have also demonstrated the usefulness of this approach in their analyses of turbulent diffusion. This approach to the study of scalar transport might be termed "statistical" since these theories require only the statistical properties of the flow field. The theories are useful for predicting the overall transport characteristics of a particle cloud, e.g., the particle mean-square displacement and eddy diffusivity. One may not, however, use them to estimate instantaneous properties of particle transport such as the instantaneous value of the particle concentration at a region in space.

For applications in which instantaneous properties of the particle concentration field are important it is necessary to incorporate information concerning the structural properties of the flow. Incorporation of the structural features of a turbulent flow field will also assist in increasing the basic understanding of particle transport and mixing. Both experimental and computational research has shown that certain regions in turbulent flow fields have significant effects on particle concentration fields. Experimental measurements of particle dispersion in free shear layers have shown that the particle concentration field is well correlated with the large-scale vortical structures in these flows (e.g., see Kobayashi *et al.*,[4] Kamalu *et al.*,[5] Lazaro and Lasheras,[6] and Longmire and Eaton[7]). For example, the experimental measurements of particle dispersion in a round jet by Longmire and Eaton have shown that dense particles collect in the saddle regions between successive vortex rings.

Analytical and computational approaches have also provided useful information concerning particle motion in turbulent flow fields. Maxey[8] used asymptotic methods to demonstrate that the effect of inertia was to cause dense particles to accumulate in regions of low vorticity and high strain rate. This bias in the particle trajectory causes a subsequent increase in the particle settling velocity over the still-fluid value. Fung and Perkins[9] have examined particle dispersion in flow fields comprised of random Fourier modes and find that for certain ratios of the particle time constant to fluid time scale it is possible that particles may become "trapped" within eddies. In a previous study of turbulence modification by particles Squires and Eaton[10] found that there was a significant effect of turbulent motions on the particle concentration fields.

Of interest in the present work is to identify which regions of turbulent flow fields significantly influence particle transport and mixing. Identification of specific regions that influence particle transport and mixing may simplify analysis of flow field dynamics and scalar mixing and should also provide insight into the development of models of turbulent flows. To this end it is necessary to have an objective set of criteria for characterizing regions of turbulent flow fields. Much of the previous work into the characterization of turbulent flow fields has been concerned with the development of criteria for defining vortical regions, i.e., regions of strong rotational motions and low pressure (e.g., see Hussain,[11] Herring,[12] Perry and Chong,[13] and Chong *et al.*[14]). Hunt *et*

 0899-8213/91/051169-10$02.00

al.[15] and Wray and Hunt[16] (hereafter denoted HWM and WH, respectively) have developed a set of criteria for defining not only vortical, or eddy, regions but also regions in which streamlines converge and the regions of relatively high-speed flow between eddies. Using the databases generated from direct numerical simulation (DNS), HWM concluded that turbulent flows can be objectively classified in terms of characteristic flow zones. HWM and WH also found that the classified flow zones contribute significantly to the overall dynamics of the flow field. One of the principal objectives of the present work is therefore to examine particle transport and mixing within the context of the flow classification technique developed by WH. Based upon their method for classifying various regions these investigators were able to deduce a characteristic structure in turbulent flow fields. Therefore, it is also desired to examine the interaction of a particle cloud with the characteristic structure defined by HWM.

II. OVERVIEW OF THE SIMULATIONS

The three-dimensional, time-dependent Navier–Stokes equations were solved for an incompressible fluid using the pseudospectral method originally developed by Rogallo.[17] This method is used to compute homogeneous turbulent flows and since homogeneous turbulence is in principle unbounded, numerical simulations of these flows employ periodic boundary conditions in a finite computational domain. Using a series representation, the velocity field is expressed as a truncated Fourier series, i.e.,

$$u_j(\mathbf{x},t) = \sum_{\mathbf{k}} \hat{u}_j(\mathbf{k},t) \exp i\mathbf{k}\cdot\mathbf{x}. \tag{1}$$

In Eq. (1) $u_j(\mathbf{x},t)$ is the jth component of the velocity in physical space and $\hat{u}_j(\mathbf{k},t)$ is the Fourier coefficient of u_j at wave vector $\mathbf{k}$. Substituting expressions such as that given by (1) into the Navier–Stokes equations and then applying the orthogonality property of $\exp i\mathbf{k}\cdot\mathbf{x}$ yields ordinary differential equations for $\hat{u}_j(\mathbf{k},t)$. An advantage of using a series representation of the dependent variables is that extremely accurate evaluation of spatial derivatives is possible because of the exponential convergence of the series (Gottlieb and Orszag[18]).

Evaluation of the nonlinear terms in a pseudospectral method is efficient since computation of these terms in physical space is less costly than in spectral or Galerkin methods. The transformation between wave-number space and physical space can be accomplished efficiently using the fast Fourier transform algorithm (Cooley and Tukey[19]). Evaluation of the nonlinear terms in physical space gives rise to aliasing errors that are eliminated in the present code using a combination of coordinate shifts and truncation. The ordinary differential equations for the Fourier coefficients are time advanced using a second-order Runge–Kutta scheme. For further details of the method see Rogallo[17] and Lee and Reynolds.[20]

A. Properties of the Eulerian field

The transport properties of dense particles were investigated using simulations of forced isotropic turbulence. For each simulation 64^3 points were used for the numerical solution of the Navier–Stokes equations. The computations were run on the Numerical Aerodynamic Simulation (NAS) facility Cray-2 supercomputer at the NASA–Ames Research Center.

Statistically stationary isotropic turbulence was achieved by artificially forcing the low wave numbers (large scales) of the velocity field using the scheme developed by Hunt *et al.*[21] At each time step of the computation a time-independent, nonuniform force is added to each of the Fourier coefficients of the fluid acceleration within a radius wave vector of $k = \sqrt{14}$. Starting from an arbitrary initial condition, a statistically stationary state is achieved after some time, in which the average rate of energy addition to the velocity field is equal to the average energy dissipation rate. To generate isotropic turbulence the moments of the force field must also satisfy isotropy. This could only be done approximately in the present computations by constraining the moments of the Fourier coefficients of the force field up to fourth order to satisfy isotropy. The force field was also constrained to be solenoidal.

The hydrodynamic properties of the flow corresponding to the statistically stationary portion of the simulation are summarized in Table I. The Reynolds number, Re_λ, in Table I is based on twice the turbulence kinetic energy and the Taylor microscale. For isotropic turbulence the Taylor microscale, λ, is given by the relation

$$\lambda = (5\nu/\epsilon)^{1/2} q. \tag{2}$$

The quantities q^2 and ϵ are twice the turbulence kinetic energy and homogeneous dissipation rate, respectively, and are determined from the three-dimensional energy spectrum:

$$\frac{1}{2} q^2 = \int_0^{k_{\max}} E(k)\,dk, \tag{3}$$

$$\epsilon = \nu \int_0^{k_{\max}} k^2 E(k)\,dk, \tag{4}$$

where k is the radial wave vector in Eqs. (3) and (4).

Another important quantity is L_f/L_{box}, the ratio of the longitudinal integral length scale to the computational box size. The integral length scale L_f is obtained by integrating the area under the correlation of longitudinal velocities, i.e.,

$$L_f = \frac{1}{\langle u_\alpha^2 \rangle} \int_0^{L_{\mathrm{box}}/2} \langle u_\alpha(\mathbf{x}) u_\alpha(\mathbf{x} + r\mathbf{e}_\alpha) \rangle\,dr \quad (\text{no sum on } \alpha). \tag{5}$$

The integral scale L_f was computed by averaging over $\alpha = 1$, 2, and 3. The computational box size L_{box} was 2π for all simulations. A dimensionless measure of the simulation res-

TABLE I. Properties of the Eulerian field from simulations of forced isotropic turbulence.

Grid	Re_λ	L_f/L_{box}	$k_{\max}\eta$	$q^3/(\epsilon L_{\mathrm{box}})$	$q^3/(\epsilon\tau_e)$
64^3	38.7	0.078	1.41	0.538	4.25

olution in Table I is $k_{max}\eta$ where k_{max} is the maximum useful wave number and η is the Kolmogorov length scale. The maximum useful wave number is determined by the dealiasing scheme and for Rogallo's code is $\sqrt{2}N/3$ where N is the number of grid points in one direction. The Kolmogorov length scale is given by the relation

$$\eta = (\nu^3/\epsilon)^{1/4}, \tag{6}$$

where ν is the kinematic viscosity of the fluid. Yeung and Pope[22] have shown that $k_{max}\eta$ should be greater than one for adequate resolution of lower-order time series statistics.

The eddy turnover time τ_e shown in Table I is estimated as

$$\tau_e = \Lambda/q, \tag{7}$$

where Λ is the length scale obtained from the three-dimensional energy spectrum, i.e.,

$$\Lambda = \frac{3\pi}{2q^2}\int_0^{k_{max}} \frac{E(k)}{k}\,dk. \tag{8}$$

The spatial energy and dissipation spectra from the simulations are shown in Fig. 1. The energy spectra at wave number k are obtained by summing the magnitudes of the Fourier coefficients falling into a wave-number band about k. These spectra were subsequently smoothed by multiplying by the ratio of the expected value of the modes in each band to the actual value contained therein (see Eswaran and Pope[23] for further details). As is evident from the figures, a distinct peak in the spectra occur where the Fourier modes are forced.

B. Particle parameters

The particle equation of motion integrated in the simulations was

$$\frac{dv_i}{dt} = \alpha\{u_i[X_j(t),t] - v_i(t)\}, \tag{9}$$

where $X_j(t)$ and $v_i(t)$ are the position and velocity of the particle, respectively. The coefficient α is the inverse of the particle response time and, assuming that the flow around the particle follows Stokes law of resistance, is given by

$$\alpha = 1/\tau_p = 18\mu/\rho_p d^2, \tag{10}$$

where μ is the dynamic viscosity of the carrier fluid, ρ_p is the particle density, and d is the particle diameter. Equation (10) is appropriate if the Reynolds number based on the relative velocity between the particle and fluid is significantly less than one. The particle is also assumed to be smaller than the smallest length scales of the flow field. For a turbulent flow this means that the particle diameter is smaller than the Kolmogorov microscale η (Maxey and Riley[24]). It is also assumed the concentration of particles is small enough such that particle–particle interactions are negligible and the turbulence is not modified by the presence of the particles. Since it is desired to examine the transport and mixing properties of dense particles suspended in turbulent flow fields the effect of an external body force has been neglected in (9).

For each simulation the Eulerian field was allowed to evolve to a statistically stationary state. Once the statistics of the hydrodynamic computation had become time independent, the particles were released in the simulation and time advanced according to Eq. (9). In order to compute statistics such as particle number density (i.e., number of particles per unit volume) it is necessary to use a large number of particles. For all of the results presented in this study the trajectories of 10^6 particles were followed. Thus, each computational volume over which the number density is defined contained, on average, 3.81 particles. Once the particles were released, the simulations were advanced slightly over six eddy turnover times. The particles were initially distributed uniformly throughout the computational volume and the initial velocity of the particle was taken to be identical to that of the fluid at the initial particle position. Because of particle inertia there is an adjustment period required for the motion of a particle to become independent of its initial velocity. Statistics were obtained only after the motion of the particles had become independent of their initial conditions. Since it is only by chance that a particle is located at a fixed grid point where the fluid velocity is calculated, vectorized trilinear interpolation was used to obtain fluid velocities at the instantaneous particle position. Numerical experiments showed that more accurate interpolation schemes do not sig-

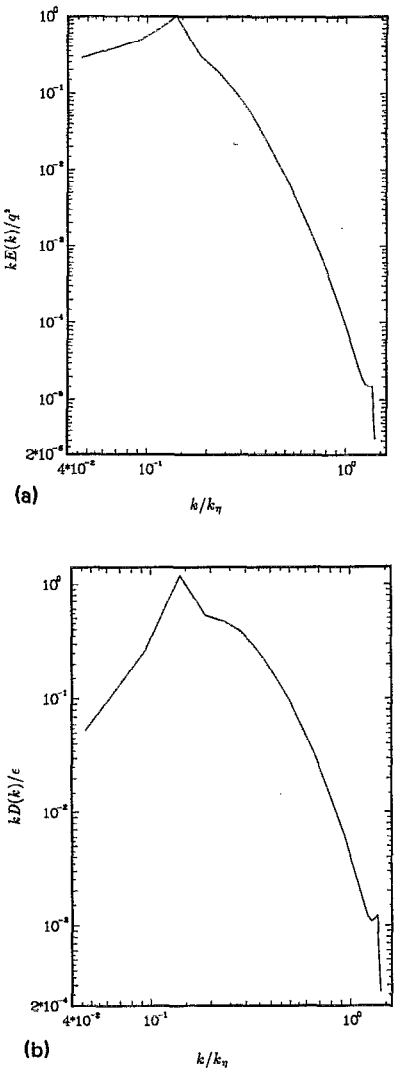

FIG. 1. Spatial spectra in forced isotropic turbulence. (a) Energy; (b) dissipation.

nificantly change the results. Since periodic boundary conditions are used for the hydrodynamic computation there is no loss of accuracy of the interpolated particle properties when the particle is near a boundary.

The properties of the particle used in the simulations are summarized in Table II. The particle time constant τ_p has been made dimensionless using the fluid time scale based on L_f and $u' = \sqrt{q^2/3}$. This time scale is denoted T_f throughout this work. The total length of time the particles were advanced in the simulations is denoted as ΔT in Table II.

III. RESULTS

The technique developed by HWM and WH for classifying zones within turbulent flow fields is summarized in Sec. III A. It is presented here for the sake of completeness since the development in Sec. III A borrows exclusively from their earlier work. The characterization of particle transport and mixing from the simulations is presented in Sec. III B.

A. Flow field classification

In their earlier work WH developed a set of criteria for classifying a turbulent flow field into four regions, or zones: eddy, convergence, stream, and rotational zones. Eddy zones are approximately defined as strong swirling regions with vorticity. In eddy zones irrotational straining is small compared to the vorticity. Thus, the second invariant of the deformation tensor is less than a negative threshold value, $-\mathrm{II}_E$:

$$\mathrm{II} < -\mathrm{II}_E, \tag{11}$$

where II is the second invariant of the deformation tensor and is defined through the relation

$$\mathrm{II} = \frac{\partial u_i}{\partial x_j}\frac{\partial u_j}{\partial x_i} = S_{ij}S_{ji} - \frac{1}{4}\omega_k\omega_k. \tag{12}$$

In Eq. (12) S_{ij} is the strain rate tensor, $\frac{1}{2}(\partial u_i/\partial x_j + \partial u_j/\partial x_i)$ and ω_k is the kth component of the vorticity vector, $\epsilon_{ijk}\,\partial u_k/\partial x_j$.

Since eddy zones are regions of rotational motion an additional criteria is that the pressure within the zone is less than a threshold value, i.e., HWM and WH used

$$p_{\mathrm{int}} < p_E, \tag{13}$$

where p_{int} is the pressure in the eddy zone and p_E is the threshold value. The criterion specified by (13) ensures that if the flow is rotational, then the streamlines are curved. Thus, nearly straight shear layers are disqualified from being classified as eddy zones.

TABLE II. Particle properties.

τ_p/T_f	$\Delta T/\tau_p$
0.075	79
0.150	40
0.520	11

Convergence zones as considered by HWM and WH are regions in which there is irrotational straining motion and strong convergence and divergence of streamlines. Such regions will contain a stagnation point. For a region to be classified as a convergence zone two conditions must be satisfied. The first criterion is that the irrotational straining is large compared with the vorticity, thus

$$\mathrm{II} > \mathrm{II}_C, \tag{14}$$

where II_C is a threshold value of II defining the convergence zone. The second criterion for a region to be classified as a convergence zone is that the pressure rises in the interior of the zone, thus

$$p_{\mathrm{int}} > p_C, \tag{15}$$

where p_{int} is the pressure in the interior of the zone and p_C is the threshold value.

Streaming zones classified by HWM and WH are regions in which the flow is relatively fast, not very curved, and not strongly convergent or divergent. The criteria proposed by WH for defining these zones are

$$u_i^2 > u_0^2 \tag{16}$$

and

$$|\mathrm{II}| < \mathrm{II}_S. \tag{17}$$

The threshold value in (17) defining the streaming zone is denoted II_S and provided that $\mathrm{II}_S = \min(\mathrm{II}_E, \mathrm{II}_C)$ no point in the field can belong to more than one zone. The criteria given above, however, are also such that not every point will be included in one of the flow zones.

A fourth zone not described by HWM but later incorporated by HW are regions possessing significant vorticity, similar to eddy zones. Unlike the circulating flow patterns of eddy zones, however, these rotational zones are regions not characterized by curved streamlines. The criterion for defining rotational zones is then

$$\mathrm{II} < -\mathrm{II}_E \tag{18}$$

which is the same criterion satisfied by the eddy zones. The pressure criteria satisfied by rotational zones are different than those satisfied by eddy zones, i.e.,

$$-p_E < p_{\mathrm{int}} < p_C. \tag{19}$$

For the results presented in this study the threshold value of II used to define convergence zones, II_C, was taken as $\mathrm{II}_C = (\overline{\mathrm{II}^2})^{1/2}$, the rms value of II from the entire flow field. For eddy zones the value of II_E was $\mathrm{II}_E = \mathrm{II}_C/2$. The threshold value of pressure used to define convergence zones, p_C, was $p_C = (\overline{p^2})^{1/2}$, the rms value of pressure from the entire flow. The value of p_E was identical to that of p_C and the value of u_0 used to define the streaming regions was $u_0 = (\overline{|\mathbf{u}|^2})^{1/2}$, the rms value of the turbulence velocity from the entire field.

HWM and WH demonstrated that the above criteria could be successfully applied to both homogeneous turbulence as well as fully developed turbulent channel flow. Application of the classification scheme to a representative plane from the present simulations is shown in Fig. 2. Superimposed on the figure are the corresponding velocity vectors. This figure shows that where the velocity vectors circle

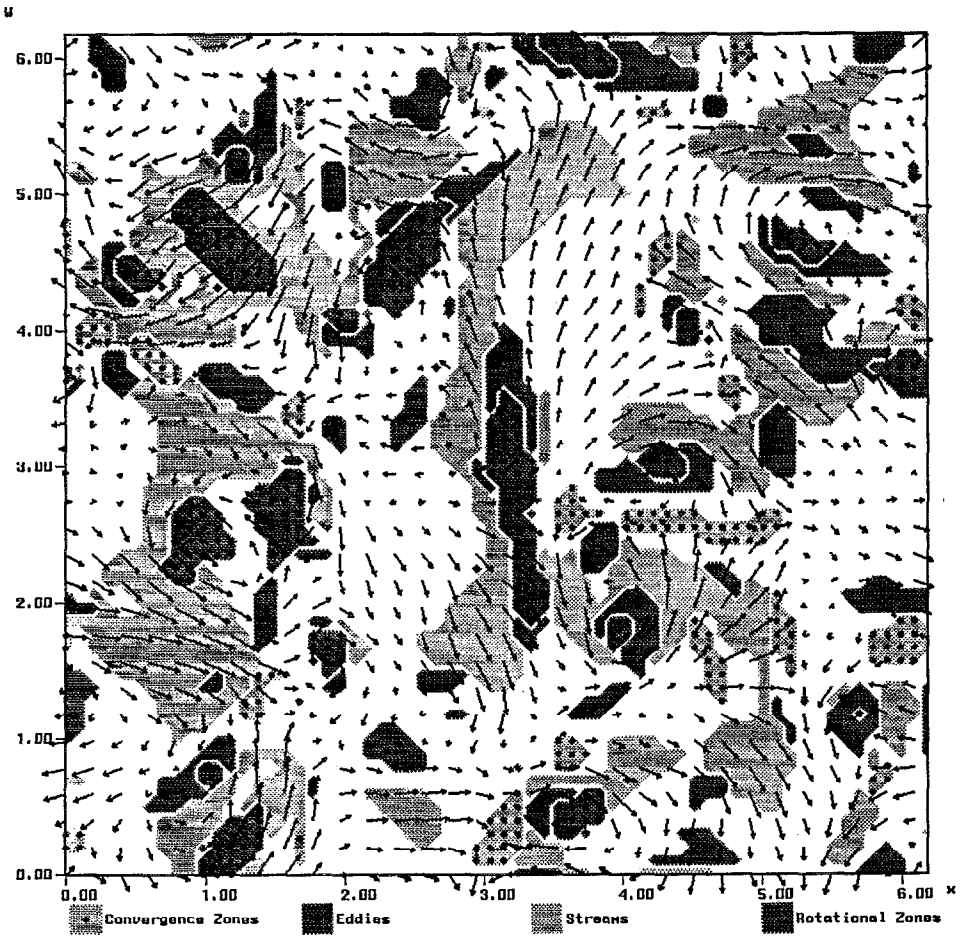

FIG. 2. Zone classification in a typical plane. Light gray with dots, convergence zones; dark gray with dots, eddy zones; light gray, stream zones; dark gray, rotational zones.

a region the zone is typically identified as an eddy. In most cases, it may be observed from the figure that rotational zones surround the eddies. The stagnation regions in the figure have been identified as convergence zones and regions in which the velocity vectors indicate high speed regions with low curvature are identified as streaming zones. Using the threshold parameters defined in the preceding paragraph approximately 53% of the domain is classified. The breakdown of the total volume is roughly as follows: 9% eddy zones, 10% rotational zones, 4% convergence zones, and 30% stream zones.

B. Properties of the particle number density field

Shown in Figs. 3(a)–3(c) are contours of the number density field in an x-y plane for each of the particle time constants used in the simulations: $\tau_p/T_f = 0.075$, $\tau_p/T_f = 0.15$, and $\tau_p/T_f = 0.52$. The contour surfaces shown in these figures correspond to identical times in the simulations and the same plane has been used for each of the figures. It is apparent from the figures that the particles are not uniformly distributed throughout the volume and there are distinct regions of particle accumulation. The peak number density in the planes shown in Figs. 3(a), 3(b), and 3(c) are 9, 25, and 10 times the mean value, respectively.

From Figs. 3(a)–3(c) it may also be observed that the nonuniformity of the concentration field is a function of the particle time constant. It is interesting to note that the effect of turbulence on the particle concentration field is not a monotonic function of the time constant. It may be seen that the greatest effect of the turbulence on the concentration field occurs for $\tau_p/T_f = 0.15$ [Fig. 3(b)]. For decreasing values of the time constant the particles behave more as fluid elements and therefore exhibit a decreasing tendency for preferential concentration [cf. Figs. 3(a) and 3(b)]. Comparison of Figs. 3(b) and 3(c) shows that as the particle time constant is increased from $\tau_p/T_f = 0.15$ to $\tau_p/T_f = 0.52$ the particles also exhibit less tendency for preferential concentration. The fact that particles with $\tau_p/T_f = 0.15$ are more preferentially concentrated than those with $\tau_p/T_f = 0.52$ is consistent with the notion that as the time constant is increased the particles become proportionately less responsive to the fluid velocity spectrum. Thus, for large enough values of the time constant it should be expected that the number density field would become uniform since extremely dense particles would not be capable of responding to the surrounding fluid velocity. It is precisely this effect which is beginning to become apparent for particles with $\tau_p = T_f = 0.52$. It is important to note, however, that evidence of structure in the number density field is apparent even for the heavier particles. Finally, the results in Figs. 3(a)–3(c) illustrate that there exists an optimum ratio of the particle time constant to fluid time scale such that particles

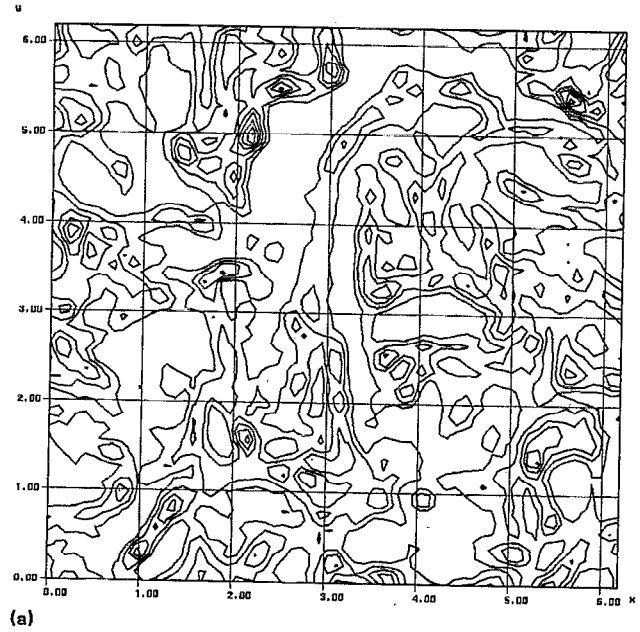

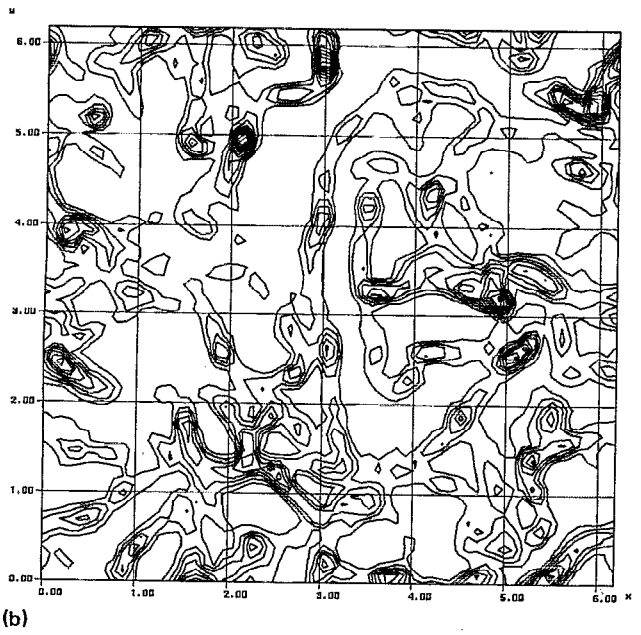

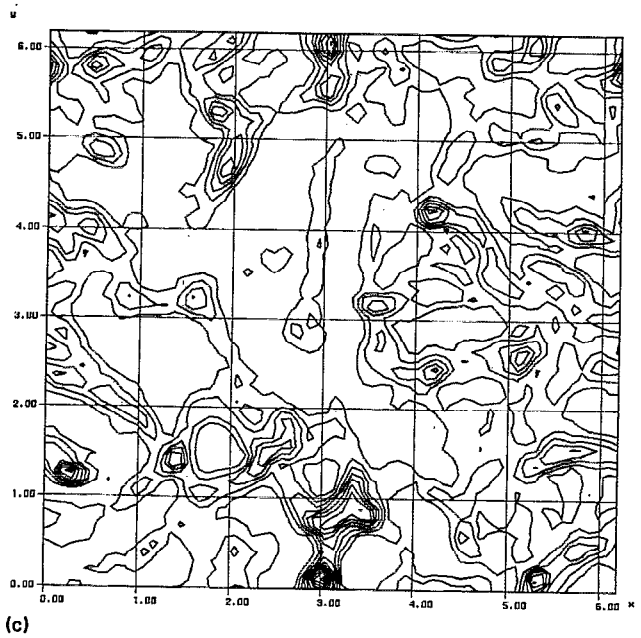

FIG. 3. Particle number density contours in an x-y plane: (a) $\tau_p/T_f = 0.075$; (b) $\tau_p/T_f = 0.15$; (c) $\tau_p/T_f = 0.52$.

will exhibit the greatest tendency for preferential concentration. For the present simulations this ratio is evidently quite close to 0.15. It should also be stressed that this conclusion is not based solely upon Figs. 3(a)–3(c). These figures are representative planes from the three-dimensional computations and the same conclusion is reached by examining the number density contours in other planes from the simulations at different times. Statistics used to quantify the effects observed in Figs. 3(a)–3(c) further corroborate the conclusion that particles with $\tau_p/T_f = 0.15$ are the most preferentially concentrated (e.g., see Fig. 6). These statistics were obtained by ensemble averaging over enough flow fields such that statistical uncertainty is small.

The classification of the flow zones in the x-y plane used in Fig. 3 is shown in each of Figs. 4(a), 4(b), and 4(c). Also shown in these figures are the particle number density contours. As can be observed from the figures, regions of high particle concentration correspond to zones in which II is large, i.e., convergence zones. The concentration of particles is also large in the streaming regions between eddies. Finally, these figures show that the particle number density is low in eddy and rotational zones. The fact that the particle concentration is low in eddy zones is consistent with physical ideas that dense particles which are within a region of swirling flow will be unable to maintain their position because of centrifugal effects. These results are also consistent with Max-

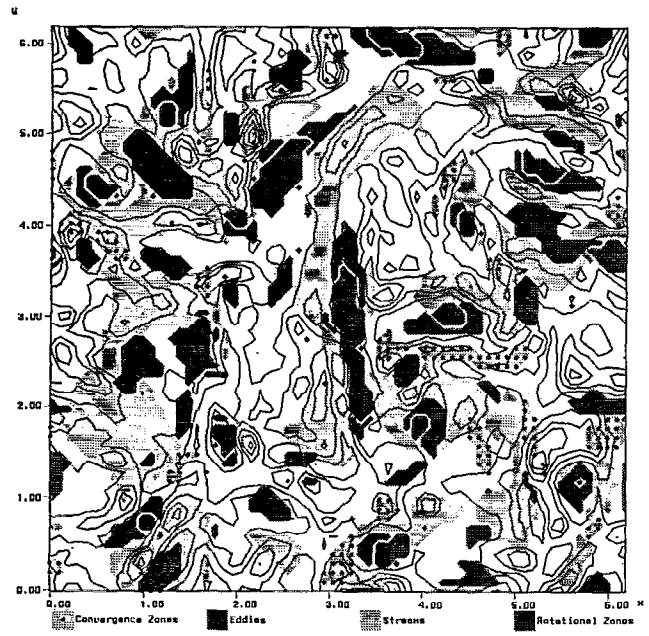

(a)

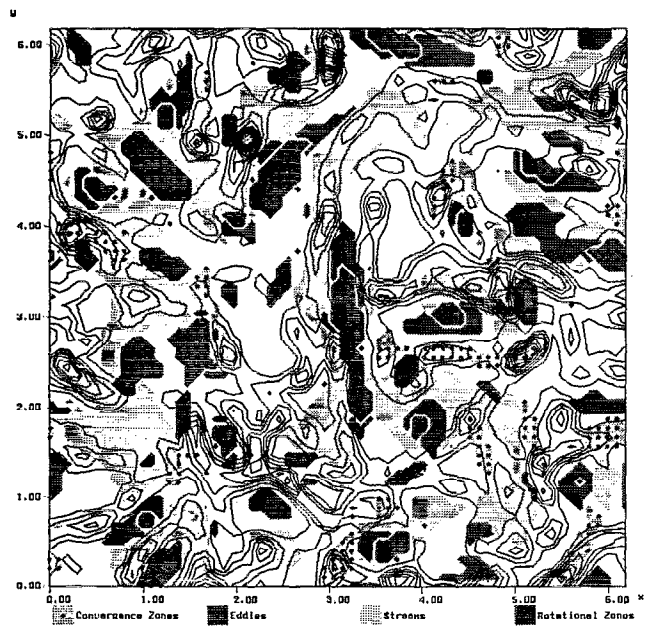

(b)

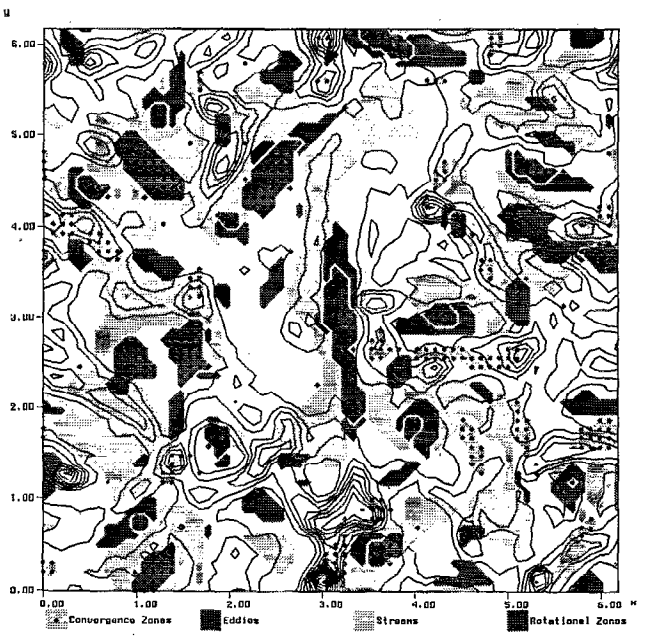

(c)

FIG. 4. Zone classification and particle number density contours, zone colors same as Fig. 2: (a) $\tau_p/T_f = 0.075$; (b) $\tau_p/T_f = 0.15$; (c) $\tau_p/T_f = 0.52$.

ey's[8] analysis which showed that the effect of inertia is to bias the particle trajectory toward regions of high strain rate (convergence zones) and low vorticity.

As mentioned in the Introduction, Fung and Perkins[9] found that for certain ratios of the particle time constant to large-scale fluid time scale particles may become "trapped" within eddies. Based upon their findings it might then be expected that particles would accumulate in eddy zones. It was not possible to verify their finding in the present work since individual time histories of the particles were not examined. Thus, while particles may become temporarily trapped in eddies (for certain ratios of the time constant to fluid time scale), it is not believed that this effect is statistically significant.

The distribution function of the particle number density provides a quantitative view of the preferential concentration observed in Figs. 3 and 4. The distribution function of the number density is shown in Fig. 5 for each of the particle

time constants along with the Poisson distribution. The Poisson distribution is given by

$$p_k = (e^{-\langle nc\rangle}/k!)\langle nc\rangle^k, \tag{20}$$

where $\langle nc\rangle$ is the mean value of the number density. The distribution function given by Eq. (20) describes the fraction of cells in the field containing k particles. The Poisson distribution results from a random distribution of the particles by the flow (e.g., see Chung[25]). The discrepancy between the measured distributions and the Poisson distribution for each of the time constants illustrates the nonuniformity of the number density field. Figure 4 shows that, for a random distribution of particles, approximately 2.5% of the cells are expected to not contain any particles. For $\tau_p/T_f = 0.15$, however, about 42% of the cells contain zero particles due to particle accumulation in regions of low vorticity and high strain rate. The figure also shows that the number of cells containing more than twice the mean number density is greater than that predicted by the Poisson distribution, again illustrating the preferential concentration of the particles by the turbulence.

As was shown in Fig. 4, the particle concentration was low in eddy zones, which are characterized by high enstrophy. This effect may be quantified by examining the conditional expectation of the number density given the value of enstrophy. This quantity is shown in Fig. 6 for each of the particle time constants and it is clear that at low values of the enstrophy the number density is greater than the mean value while for higher values of the enstrophy the number density is decreased relative to the mean. Figure 6 also demonstrates that particles with $\tau_p/T_f = 0.15$ are the most responsive to turbulent motions, i.e., at low values of the enstrophy the number density for these particles is greater than that for $\tau_p/T_f = 0.075$ or $\tau_p/T_f = 0.52$. At higher values of the enstrophy the number density for particles with $\tau_p/T_f = 0.15$ is less than that of the other two time constants.

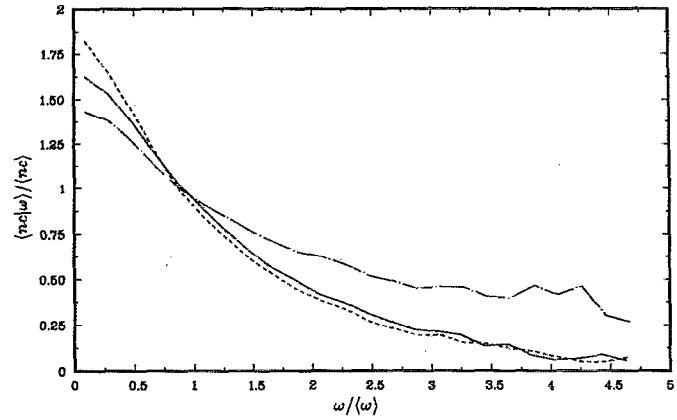

FIG. 6. Conditional expectation of the number density given enstrophy: —, $\tau_p/T_f = 0.075$; ----, $\tau_p/T_f = 0.15$; -·-, $\tau_p/T_f = 0.52$.

The average particle number density within each of the zones described in Sec. III A is shown in Fig. 7. The zone-averaged number density $\langle nc_z\rangle$ shown in this figure has been made dimensionless using the mean number density computed from the entire field, $\langle nc\rangle$. Consistent with both the physical arguments discussed earlier as well as Maxey's[8] analysis, the particle number density is smallest in the eddy zones and largest in the regions identified as convergence zones. It is important to remember that if the particles were randomly distributed, then the zone-averaged number density would be identical to the global mean and the four values of $\langle nc_z\rangle$ for a given time constant would collapse to a single point (the global mean). This is presumably the effect that can be observed as the time constant is increased in Fig. 7, though values of τ_p/T_f much larger than 0.52 may be required for this effect to become significant. The largest value of the zone-averaged number density is seen to occur for

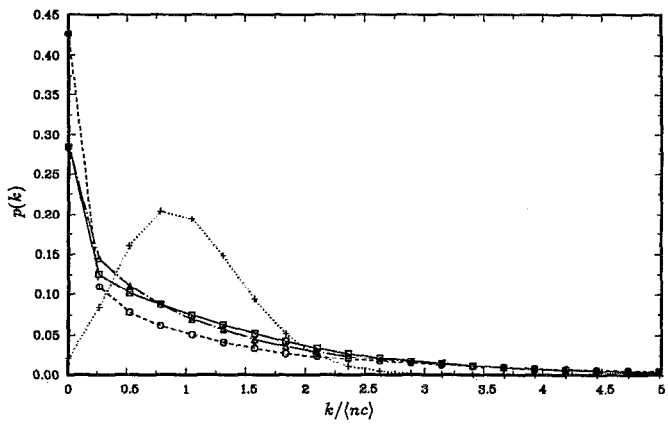

FIG. 5. Particle number density distribution function: □—□, $\tau_p/T_f = 0.075$; -○-, $\tau_p/T_f = 0.15$; -△-, $\tau_p/T_f = 0.52$; + ··· +, Poisson distribution.

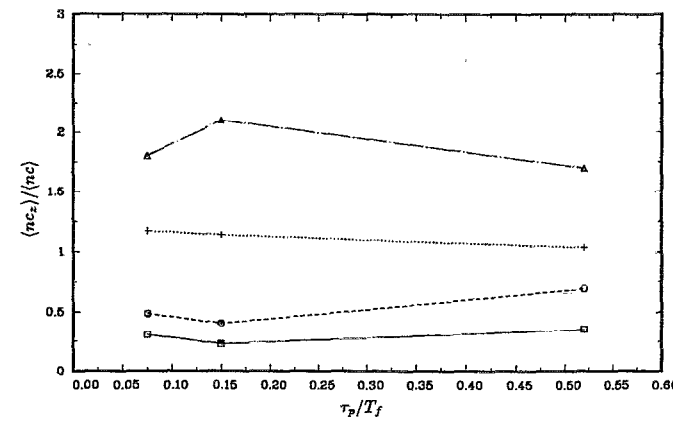

FIG. 7. Zone-averaged particle number density: □—□, eddy; -○-, rotational; -△-, convergence; + ··· +, stream.

$\tau_p/T_f = 0.15$ in the convergence zones and is over twice the global mean number density. This helps to further illustrate that these particles exhibit the greatest tendency for preferential concentration.

The fraction of the total number of particles contained within each flow zone is shown in Fig. 8. Figure 8 clearly shows that the fraction of particles contained within the stream zones is substantially greater than those in the eddy, rotational, or convergence zones. It can be observed in Fig. 8 that, depending on the time constant, the fraction of particles contained in the stream zones is between 31% and 36% of the total. Since the average number density in these zones is slightly greater than the global mean (see Fig. 7), the fraction of particles contained in the stream zones will be slightly larger than the volume occupied by these zones. For the threshold parameters used in these computations the stream zones occupy the largest volume of the classified domain, approximately 30%. Thus, it is not surprising that the largest fraction of particles are within stream zones. Figure 8 also shows that the fraction of particles contained within the convergence zones is between 7% and 9% of the total. Though this is a rather small fraction of the total number of particles, it is important to remember that the average number density in these regions is as much as twice the global mean (see Fig. 7). Thus, the fraction of the total number of particles contained within convergence zones is proportionally greater than the volume occupied by these zones. It is also interesting to note from Fig. 8 that while the fraction of particles contained within the stream zones decreases monotonically with increasing time constant, the fraction of particles within the convergence zones shows a slight maximum for $\tau_p/T_f = 0.15$. This is presumably due to the fact that these particles exhibit the greatest tendency for preferential concentration.

Another interesting result from the simulations is the mean-square relative velocity between fluid and particles in each of the zones. This quantity is shown in Fig. 9 and it may be observed from the figure that the mean-square velocity difference is greatest in the convergence zones. WH found

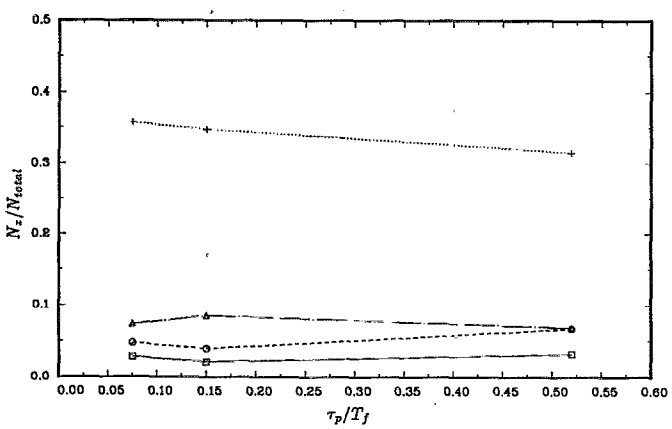

FIG. 8. Fraction of particles contained within flow zones: □—□, eddy; –○–, rotational; –△–, convergence; + ··· +, stream.

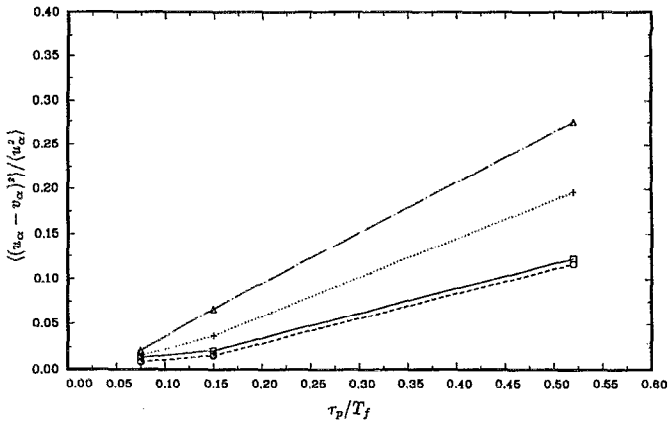

FIG. 9. Zone-averaged mean-square relative velocity. □—□, eddy; –○–, rotational; –△–, convergence; + ··· +, stream.

that the contribution of the convergence zones to the kinetic energy of the flow was less than their volume fraction. Thus, the convergence zones are relatively low-speed regions and this contributes to the increase in the velocity difference between particles and fluid. An additional effect increasing the velocity difference between particles and fluid in these regions is particle inertia. As dense particles move into these regions they are not able to decelerate as quickly as the fluid and this acts to further amplify the velocity difference in these zones. It was found that, for a given time constant, the velocity difference between particles and fluid in the convergence and stream zones was greater than the global value while the mean-square velocity difference in the eddy and rotational zones was less than the velocity difference computed from the entire field. This result that the mean-square velocity difference is greatest in the convergence and stream zones is directly relevant to problems such as turbulence modification by dense particles. For particles whose motion is governed by Stokes drag, the source term in the Navier–Stokes equations representing turbulence modification by particles is proportional to the velocity difference between the fluid and particles and the local particle concentration. Based on these results, it should be expected that the convergence and stream zones will be modified much differently than the eddy or rotational zones.

IV. SUMMARY AND CONCLUSIONS

Results from simulations of forced isotropic turbulence show that there is a significant effect of turbulence structure on the concentration fields of dense particles. In agreement with Maxey's[8] analysis it was found that particle inertia causes a bias in the trajectory toward regions of low vorticity and high strain rate. Instantaneous values of the particle number density were as much as 25 times the mean value in these regions. The preferential concentration of particles by turbulence has interesting implications concerning the mixing of dense particles in turbulent flow fields. Conventional thinking that views particle mixing by turbulence as a homogeneous process in which particles are uniformly dispersed by the turbulence can be grossly in error. It has been demon-

strated that the mixing of particles by turbulence is strongly dependent upon the relative time scales of the two phases. For certain ratios of τ_p/T_f the turbulence may "de-mix" the particles (see also Ottino[26]).

The flow classification scheme of HWM and WH helps to clarify particle transport and mixing in turbulent flows. In their previous work HWM deduced that the characteristic three-dimensional structure consistent with the flow zones defined in Sec. III A was one of vortex lines concentrating in smaller regions into vortex tubes. These vortices induce motion in each other and produce stream zones between the vortices. Convergence zones occur where stream zones meet one another. Particle transport and mixing consistent with this three-dimensional structure is that particles move through the flow via the streaming zones. Since the stream zones often terminate into other streaming zones to produce convergence zones, one should expect that the number density in these regions will be greater than the global mean number density (see Sec. III B and Fig. 7).

ACKNOWLEDGMENTS

The authors are grateful to Dr. Robert Rogallo of the NASA–Ames Research Center for the use of his code. The authors are also indebted to Dr. Alan Wray of the NASA–Ames Research Center for assistance with the VECTORAL compiler as well as the use of his flow field kinematics program.

This work was supported by the NASA/Stanford Center for Turbulence Research and the National Science Foundation Fluid Dynamics Program (Grant No. MEA-83-51417).

[1] G. I. Taylor, Proc. R. Soc. London Ser. A **20**, 196 (1921).
[2] G. K. Batchelor, Aus. J. Sci. Res. **2**, 437 (1949).
[3] S. Corrsin, *Proceedings of the Iowa Thermodynamics Symposium* (University of Iowa, Iowa City, Iowa, 1953), pp. 5–30.
[4] H. Kobayashi, S. M. Masutani, S. Azuhata, N. Arashi, and Y. Hishinuma, *Transport Phenomena in Turbulent Flows*, edited by M. Hirata and N. Kasagi (Hemisphere, New York, 1988), pp. 433–446.
[5] N. Kamalu, L. Tang, T. R. Troutt, J. N. Chung, and C. T. Crowe, *International Conference on Mechanics of Two-Phase Flows* (National Taiwan University, Taipei, Taiwan, 1989), pp. 199–202.
[6] B. J. Lazaro and J. C. Lasheras, Phys. Fluids A **1**, 1035 (1989).
[7] E. K. Longmire and J. K. Eaton, *Proceedings of the Korea–U.S. Fluids Engineering Seminar*, edited by J. Kim (Korea Institute of Technology, Taejon, Korea, 1989), pp. 435–454.
[8] M R. Maxey, J. Fluid Mech. **174**, 441 (1987).
[9] J. Fung and R. J. Perkins, *Proceedings Advances in Turbulence 2*, edited by H. Fernholz and H. Fielder (Springer, New York, 1989).
[10] K. D. Squires and J. K. Eaton, Phys. Fluids A **2**, 1191 (1990).
[11] A. K. M. F. Hussain, J. Fluid Mech. **173**, 303 (1986).
[12] J. Herring, Proceedings of the 17th International Congress on Theoretical and Applied Mechanics, Grenoble, 1988.
[13] A. E. Perry and M. S. Chong, Annu. Rev. Fluid Mech. **19**, 125 (1987).
[14] M. S. Chong, A. E. Perry, and B. J. Cantwell, Phys. Fluids A **2**, 765 (1990).
[15] J. C. R. Hunt, A. A. Wray and P. Moin, Proceedings of the CTR Summer Program, 1988, pp. 193–208.
[16] A. A. Wray and J. C. R. Hunt, Proceedings of the IUTAM Topology of Fluid Mechanics, Cambridge, 1989, pp. 95–104.
[17] R. S. Rogallo, NASA Tech. Memo. 81315 (1981).
[18] D. Gottlieb and S. A. Orszag, *Numerical Analysis of Spectral Methods: Theory and Applications*, CBMS–NSF Regional Conference Series in Applied Mathematics (SIAM, Philadelphia, PA, 1977), Vol. 26.
[19] J. W. Cooley and J. W. Tukey, Math. Comput. **19**, 297 (1965).
[20] M. J. Lee and W. C. Reynolds, Department of Mechanical Engineering Report No. TF-24, Stanford University, Stanford, California, 1985.
[21] J. C. R. Hunt, J. C. Buell, and A. A. Wray, *Proceedings of the 1987 Summer Program* (Stanford University, Stanford, CA, 1987), Report No. CTR-S87.
[22] P. K. Yeung and S. B. Pope, J. Comput. Phys. **79**, 373 (1988).
[23] V. Eswaran and S. B. Pope, Comput. Fluids **16**, 257 (1988).
[24] M. R. Maxey and J. J. Riley, Phys. Fluids **26**, 883 (1983).
[25] K. L. Chung, *Elementary Probability Theory with Stochastic Processes* (Springer, New York, 1975).
[26] J. O. Ottino, Annu. Rev. Fluid Mech. **22**, 207 (1990).